Sensors and Materials, Vol. 37, No. 7 (2025) 3061–3072
MYU Tokyo

S & M 4103

Multiscale Window Analysis for Enhanced Detection of Sea Ice in Liaodong Bay Using Geostationary Ocean Color Imager-II and Sentinel-2 Data

Kwangseok Kim,[1*] Min-Kyu Kim,[2] Young-Je Park,[3] Hyun Yang,[4]
Hyeong-Tak Lee,[1] Hee-Jeong Han,[1] Suk Yoon,[1] and Jeong-Eon Moon[1]

[1]Korea Institute of Ocean Science and Technology, Korea Ocean Satellite Center,
385 Haeyang-ro, Yeongdo-gu, Busan 49111, Republic of Korea
[2]Korea Institute of Ocean Science and Technology, Maritime Robotics Test & Evaluation Center,
1104, Haean-ro, Heunghae-eup, Buk-gu, Pohang-si, Gyeongsangbuk-do 37553, Republic of Korea
[3]TelePIX Co., Ltd., NongHyup Foundation Building,
2, International Finance Road 8-gil, Yeongdeungpo-gu, Seoul 07330, Republic of Korea
[4]Korea Maritime and Ocean University, Division of Maritime AI & Cyber Security,
727 Taejong-ro, Yeongdo-gu, Busan 49112, Republic of Korea

(Received December 31, 2024; accepted June 27, 2025)

Keywords: sea ice detection, multiscale window analysis, satellite data, GOCI-II, deep learning

Sea ice should be detected accurately to mitigate risks to marine industries, protect coastal infrastructure, and understand the dynamic interactions between sea ice and the marine environment. In this study, we developed and validated a sea ice detection algorithm based on a multilayer perceptron (MLP) for the Bohai Sea using Geostationary Ocean Color Imager-II (GOCI-II) and Sentinel-2 data. High-resolution Sentinel-2 imagery generates the sea ice truth data, which are then resampled to align with the GOCI-II grid. Rayleigh-corrected reflectance data from GOCI-II are used as input variables for the MLP algorithm. Multiscale Window Analysis enhances detection accuracy and reduces the false detections inherent in pixel-based approaches. The performance of the detection algorithm is evaluated using different window sizes (1 × 1, 3 × 3, 5 × 5, 7 × 7, and 9 × 9 pixels). The results demonstrate that increasing the window size enhances performance metrics, underscoring the importance of incorporating the surrounding reflectance variations in sea ice detection. Additionally, the developed algorithm was applied to hourly GOCI-II images for further analysis. A qualitative evaluation confirmed that sea ice was successfully detected, and the algorithm effectively identified the temporal movement of sea ice.

1. Introduction

Sea ice plays a critical role in climate systems and marine environments by modifying surface reflectivity, which impacts regional weather patterns and energy balance.[1–3] Beyond its environmental impact, sea ice exerts economic influence. Floating sea ice disrupts aquaculture

*Corresponding author: e-mail: kwangseok@kiost.ac.kr
https://doi.org/10.18494/SAM5644

ISSN 0914-4935

and fisheries, obstructs maritime transportation, and damages offshore infrastructure (such as oil platforms), leading to considerable financial losses.[4–6] Consequently, sea ice distribution and movement should be monitored and detected accurately to protect marine ecosystems and minimize economic risks.

Satellite remote sensing is indispensable for large-scale sea ice monitoring. Previous studies have demonstrated the utility of various satellite technologies for detecting and analyzing sea ice in the Bohai Sea. Several researchers used synthetic aperture radar to detect sea ice.[4,7,8] Others utilized polar-orbiting satellites, such as the Moderate-Resolution Imaging Spectroradiometer and the Advanced Very-High-Resolution Radiometer, for their broad spatial coverage.[2,9–12] Moreover, geostationary satellites, such as the Geostationary Ocean Color Imager-II (GOCI-II), provide high temporal resolutions, enabling the effective observation of sea ice dynamics.[13–16]

The sea ice in the Bohai and Yellow seas is characterized by rapid spatial and temporal variations, with thin ice layers and complex optical properties. High turbidity in seawater complicates detection.[17] These challenges can be overcome using monitoring strategies that integrate datasets with high spatial and temporal resolutions. Although polar-orbiting satellites offer broad coverage, their low temporal resolution limits their effectiveness for real-time monitoring. By contrast, geostationary satellites provide high temporal resolutions and are better suited for tracking dynamic phenomena, such as sea ice in the Bohai Sea.[13]

GOCI-II is particularly advantageous for sea ice monitoring, providing hourly observations over a wide spatial range. This enables the effective tracking of the dynamic changes in the sea ice distribution in the Bohai and Yellow seas.[14,15] Sentinel-2 offers a high spatial resolution of 10 m, allowing detailed analyses of the regional features of sea ice. Combining the temporal resolution of GOCI-II with the spatial accuracy of Sentinel-2 can lead to the development of more robust and precise sea ice detection methodologies. Multiscale window analysis (MWA) can further enhance detection accuracy by incorporating surrounding spatial information. Integrating MWA into a sea ice detection algorithm can improve the reliability of sea ice monitoring. This approach may significantly enhance the efficiency of sea ice monitoring and provide valuable insights for environmental management and maritime safety in these regions.

2. Study Area and Materials

The Bohai Sea, a semi-enclosed area in the northern Yellow Sea, has an average depth of only 18 m and is the world's southernmost region where sea ice forms.[15] This region is economically significant owing to its proximity to Beijing, the capital of China, high maritime traffic, and abundant oil and natural gas resources. Thus, the sea ice in the Bohai Sea considerably affects marine transportation, fisheries, port facilities, and oil and gas exploration.[14,15]

Within the Bohai Sea, sea ice formation occurs the earliest and lasts the longest in Liaodong Bay (Fig. 1), where it typically persists from December to the following March. High temporal resolutions in ice monitoring are essential to minimize damage risks to port and offshore facilities, such as oil platforms. In particular, the spatial distribution and thickness of sea ice should be monitored to maintain environmental stability and minimize economic losses in this

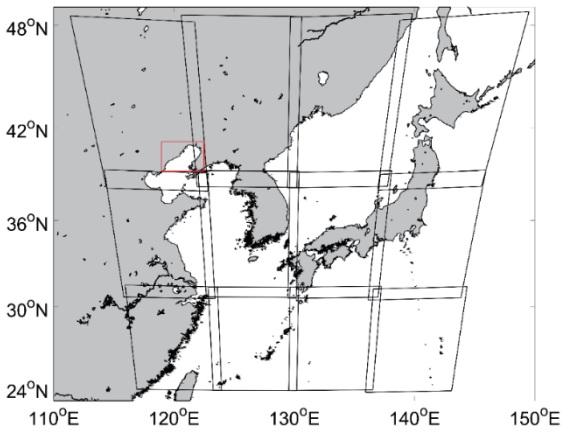

Fig. 1. Study area. The black and red solid box outlines indicate the GOCI-II observation and study areas, respectively.

region. Because a large amount of sea ice in the Bohai Sea is floating, tracking drift ice is also essential, as demonstrated by a previous study[13] that validated the utility of GOCI hourly imagery for monitoring sea ice movement in this area.

In this study, we used data from GOCI-II, the next-generation GOCI, and Sentinel-2 satellite imagery to detect and validate sea ice in the Liaodong Bay. GOCI-II observes the Northeast Asian region, including the Korean Peninsula, Japan, China, and other nearby areas (Fig. 1), at a spatial resolution of approximately 300 m (Table 1). The sensor conducts observations 10 times a day at 1 h intervals, from 8 AM to 5 PM (local time), providing the advantage of monitoring the short-term variability of ocean phenomena within the observation area. Sentinel-2 provides high-resolution imagery suited for observing detailed ice features. A convergence study using these satellites will enhance the efficiency of real-time sea ice monitoring and detection.

In this study, we used images from the 2021 sea ice season, the only period when GOCI and GOCI-II were observing simultaneously. Sentinel-2 level-2A data were acquired from the Copernicus browser (https://browser.dataspace.copernicus.eu), whereas GOCI-II level-2 data corresponding as closely as possible to the Sentinel-2 observation times were obtained from the National Ocean Satellite Center (https://www.nosc.go.kr/main.do).

3. Methods

3.1 Multilayer perceptron (MLP)

An MLP is a widely used artificial neural network model that extends the capabilities of a single-layer perceptron, first proposed by Frank Rosenblatt in 1957.[18,19] Although single-layer perceptrons can solve simple linear classification problems, their lack of hidden layers prevents them from addressing more complex, nonlinear tasks, such as the exclusive OR problem. An MLP overcomes these limitations using one or more hidden layers incorporated between its input and output layers, enabling it to model nonlinear relationships and predict continuous

Table 1
GOCI-II and Sentinel-2 specifications.

Sensor	GOCI-II	Sentinel-2
Temporal resolution	1 h	10 days (each single satellite)
Revisit period	10 times/day, 8 AM–5 PM (KST)	5 days (combined constellation)
Spatial resolution	300 m/pixel	10 to 60 m, depending on band
Bands	12 visible and NIR bands, 1 wideband	10 visible and NIR bands, 3 SWIR bands

functions.[20,21] This makes MLPs suitable for applications such as pattern classification, prediction, and regression.

In this study, an MLP model was developed to predict the presence of sea ice using Rayleigh-corrected reflectance (RRC) data from 12 GOCI-II bands. The designed MLP architecture includes four fully connected hidden layers, with 256, 128, 64, and 32 neurons in the first to fourth layers, respectively (Fig. 2).[22] A rectified linear unit activation function was applied per layer, and a softmax activation function was used in the output layer to generate probability distributions, enabling the classification of the presence of sea ice. A categorical cross-entropy loss function was used to measure the difference between the predicted and actual probability distributions. Then, an Adam optimizer was used to minimize the value of the loss function during training.

To further improve the detection accuracy, we enhanced the model to account for surrounding pixels in addition to the target pixel. Instead of using only the 12 RRC values for a single pixel, this method considers the RRC values of neighboring pixels (additional details in Sect. 3.2). This approach leverages the spatial context to refine predictions, addressing potential errors caused by local variations in reflectance and improving the robustness of sea ice detection.

3.2 Data processing

Sea ice ground truth data are essential for sea ice detection using MLPs. In this study, high-spatial-resolution Sentinel-2 imagery was visually analyzed to create the ground truth data, categorizing the study area into sea ice, nonsea ice, and ambiguous regions (Fig. 3). Ambiguous regions refer to areas where sea ice coverage is small or the ice is thin, making it difficult to definitively classify them as either sea ice or nonsea ice. These regions predominantly occur along sea ice boundaries. Since the MWA method is used, adjacent water areas surrounding the sea ice were also included in the ambiguous region category to account for spatial variability. In the subsequent analysis, only the sea ice and nonsea ice areas were utilized, and the Sentinel-2-based ground truth data were reprojected to match the GOCI-II ground truth data.

For sea ice detection, we used RRC data from 12 bands of GOCI-II. The mean and standard deviation for each band within the study area were calculated, and outliers (values beyond two standard deviations from the mean) were removed. Then, the data per area were normalized by dividing them by the minimum value within that area. The numbers of sea ice and nonsea ice data used in the MLP were balanced by conducting random sampling from the larger dataset (nonsea ice dataset). The final dataset was divided into training and validation data in a 3:1 ratio.

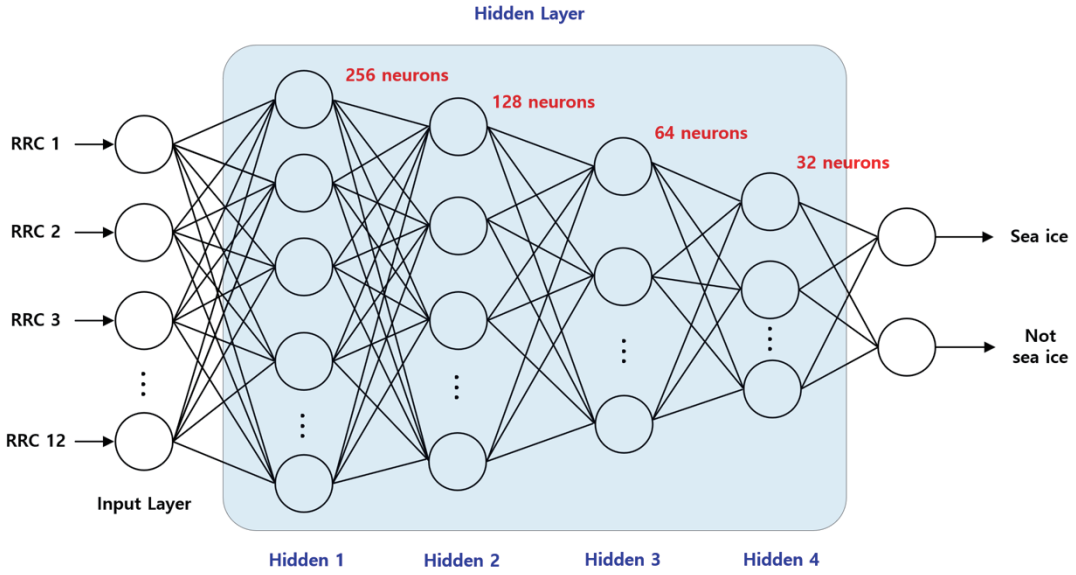

Fig. 2. (Color online) Structure of the MLP used in this study.

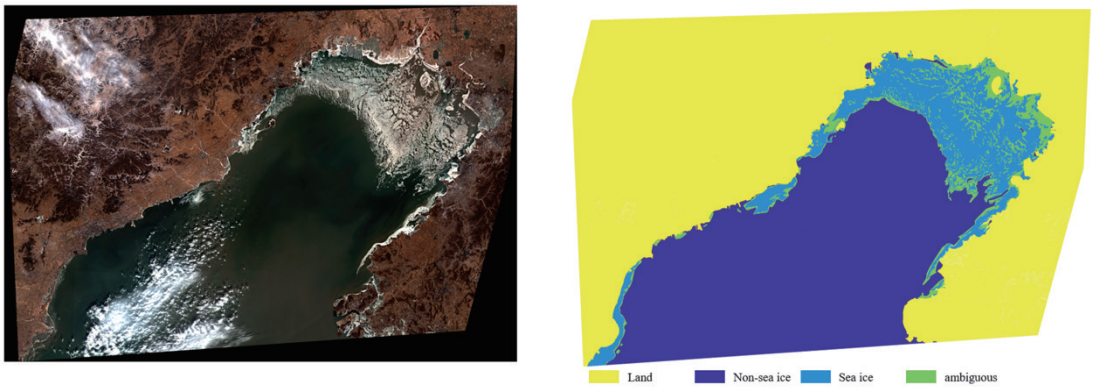

(a) (b)

Fig. 3. (Color online) (a) Sentinel-2 RGB image and (b) ground truth data (January 1, 2021).

The use of a 3 × 3 standard deviation filter can enhance the separation of sea ice from seawater.[15] In this study, MWA was used to examine the accuracy of sea ice detection based on the window size.

4. Results

4.1 Validation

In the performance validation of the MLP model, the ground truth data derived from Sentinel-2 on January 1, 2021 were resampled to match the GOCI-II grid. The dataset was used

for training and validating the MLP-based sea ice detection approach. For each window size (1, 3, 5, 7, and 9), 10 independent MLP models were trained, resulting in a total of 50 models. Each trained model was then validated using a separate test dataset. During training, any window containing invalid pixel values (e.g., missing or erroneous data) was excluded to maintain high data quality. As the window size increased, the numbers of valid pixels for the sea ice and nonsea ice classes decreased owing to the higher probability of encountering invalid pixels within larger windows (Table 2).

Table 2 presents the results of applying the 50 models to the validation dataset. With an increase in window size, certain model performance metrics consistently improved, such as accuracy, precision, and F1-score. The F1-score had a minimum value of 0.9600 at the window size of 1 and peaked at 0.9807 at the window size of 7. However, the F1-score slightly declined at the window size of 9, suggesting potential limitations in performance improvement at overly large window sizes. Therefore, utilizing a broader spatial context through larger window sizes enhances the model's ability to distinguish between sea ice and nonsea ice regions, and excessively large windows may lead to saturation, limiting further improvements.

4.2 Test

The performance of the developed sea ice detection models (Sect. 4.1) was tested. The Sentinel-2 imagery acquired on February 17, 2021 was selected for testing owing to its favorable air quality, extensive sea ice coverage, and wide nonsea ice area. The results, summarized in Table 3, indicate that the performance metrics increased with the window size, consistent with the validation phase. The recall metric peaked at the window size of 7, as in the validation

Table 2
Validation results (averaged results from 10 models).

Window size	No. of nonsea ice data	No. of sea ice data	True positive (TP)	False negative (FN)	False positive (FP)	True negative (TN)	Accuracy	Precision	Recall	F1-score
1	178865	50264	12068	498	508	12058	0.9600	0.9596	0.9604	0.9600
3	172974	50084	12221	300	276	12245	0.9770	0.9779	0.9761	0.9770
5	167275	49873	12156	312	145	12323	0.9817	0.9882	0.9749	0.9815
7	162433	49618	12146	258	220	12184	0.9807	0.9822	0.9792	0.9807
9	158337	49335	11981	353	218	12116	0.9768	0.9822	0.9714	0.9767

Table 3
Test results obtained using GOCI-II data on February 17, 2021.

Window size	No. of nonsea ice data	No. of sea ice data	TP	FN	FP	TN	Accuracy	Precision	Recall	F1-score
1	5464	42216	35297	6919	5182	282	0.7462	0.8715	0.8361	0.8524
3	3905	36158	34291	1867	3375	530	0.8692	0.9104	0.9484	0.9285
5	2824	30648	29210	1438	2063	761	0.8954	0.9345	0.9531	0.9433
7	2007	26047	25610	437	1311	697	0.9377	0.9513	0.9832	0.9670
9	1458	22358	21906	453	592	866	0.9561	0.9740	0.9798	0.9767

results, whereas the other metrics achieved their highest values at the window size of 9. Although the test results were slightly lower than the validation results, they still demonstrated excellent performance. Specifically, the F1-score increased from 0.8524 at the window size of 1 to 0.9767 at the window size of 9.

Figure 4 illustrates the spatial distribution of false negatives (FNs) and false positives (FPs) for each window size. The color bar represents the frequencies of FN and FP occurrences throughout 10 model runs. The results indicate that areas with dense sea ice exhibited minimal false detections, whereas FNs and FPs were predominantly observed near the edges of sea ice and in nonsea ice regions.

The MLP-based sea ice detection algorithm developed in this study, utilizing 9 × 9 window analysis, was applied to GOCI-II imagery for further analysis. Since small solar zenith angles in the early morning and late afternoon during winter can affect image quality, only the data acquired between 10 AM and 2 PM (local time) were utilized. Images from 9 AM were excluded from the analysis owing to the absence of observations in the study area caused by the wheel offloading of the satellite. Figure 5 presents the results of sea ice detection using GOCI-II imagery. The left panels display RGB images at 1 h intervals, while the right panels overlay the detected sea ice regions on the corresponding RGB images. The detection results were determined on the basis of predictions from 10 different models, where a given area was

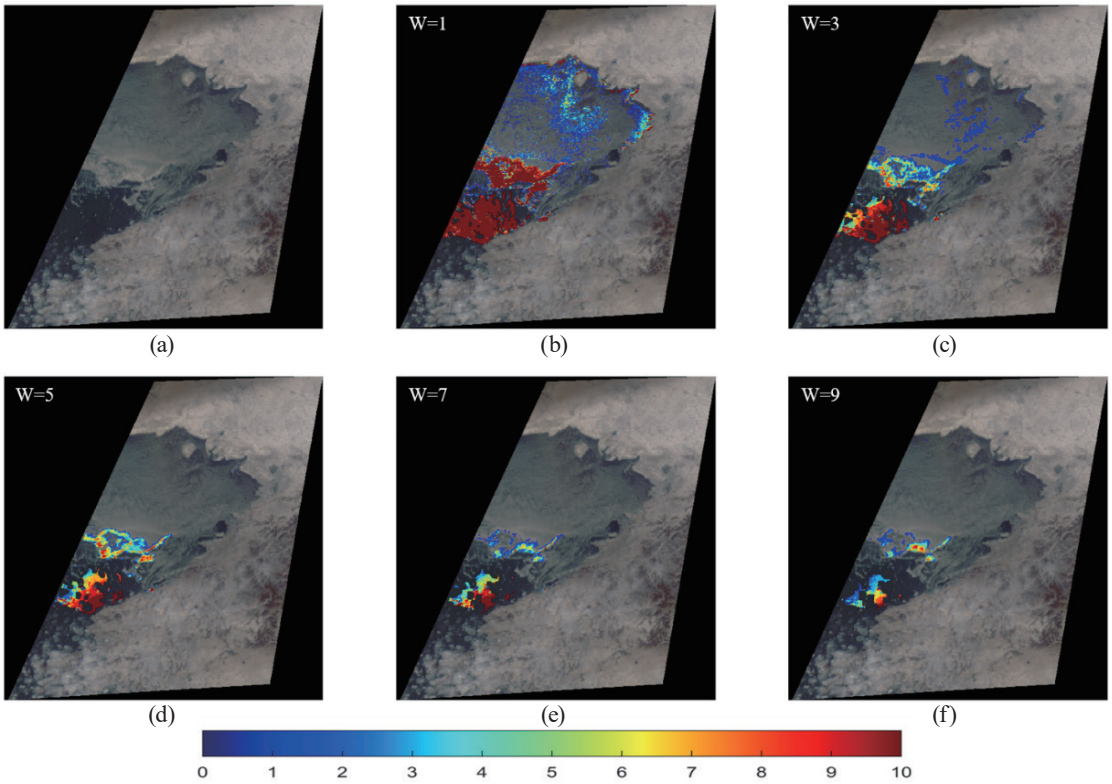

Fig. 4. (Color online) (a) RGB image and (b)–(f) FN and FP locations according to window size (from 1 to 9) on February 17, 2021.

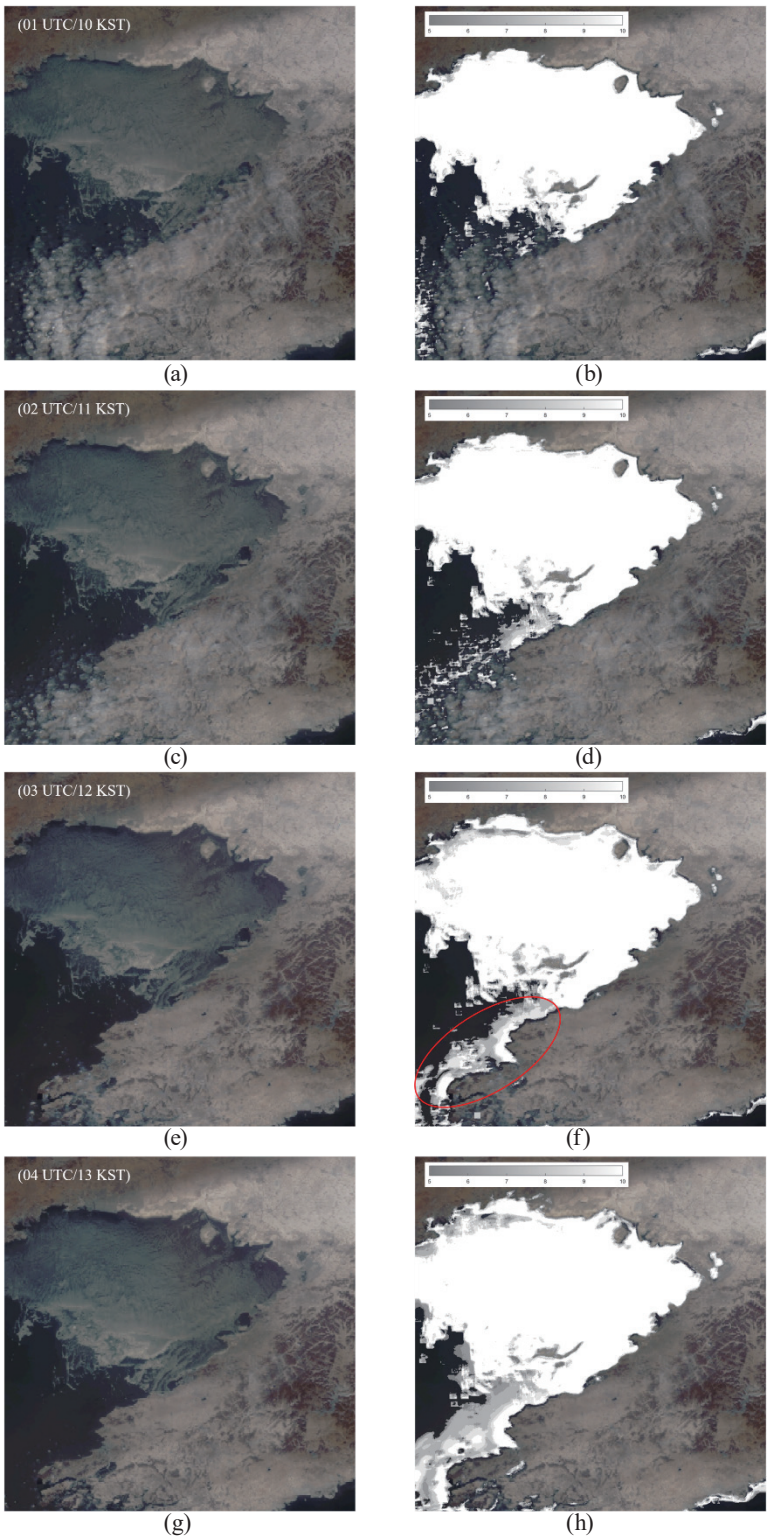

Fig. 5. (Color online) RGB images (left) and sea ice detection results overlaid on RGB images (right) from 10 AM to 2 PM (local time) on February 17, 2021.

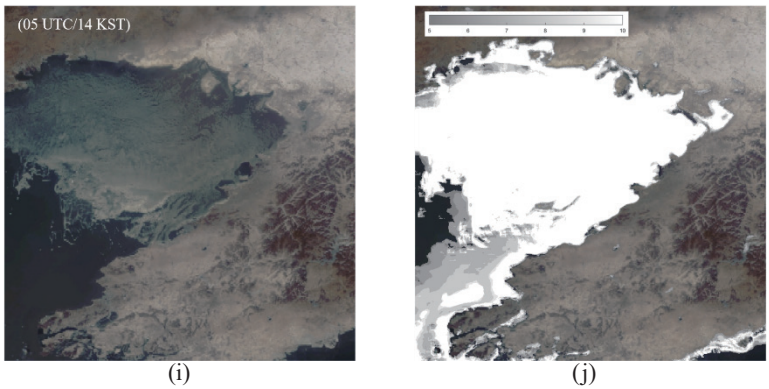

(i) (j)

Fig. 5. (Continued) (Color online) RGB images (left) and sea ice detection results overlaid on RGB images (right) from 10 AM to 2 PM (local time) on February 17, 2021.

classified as sea ice if at least five models identified it as such. Since ground truth data were not available for each image, a quantitative accuracy assessment was not conducted. However, the results indicate that the algorithm successfully detected sea ice in areas where it was expected to be present. Notably, nearly all models consistently classified sea ice regions as sea ice (refer to the color bar for details of the areas shown in white). Furthermore, as time progressed, sea ice drifted southwestward away from the coastline owing to tidal currents. However, from 11 AM onward, an increasing number of false detections along the southern coastline [shown by the red elliptical region in Fig. 5(f)] of the study area were observed. The underlying cause of this phenomenon requires further investigation in future studies.

5. Conclusions and Discussion

In this study, we developed and evaluated MLP-based sea ice detection algorithms for the Bohai Sea using GOCI-II and Sentinel-2 data. The sea ice ground truth data, derived from high-resolution Sentinel-2 imagery, were resampled to align with the GOCI-II grid. RRC data from GOCI-II were then used as input variables for the MLP algorithm. MWA was adopted to overcome the limitations of pixel-based detection methods and enhance detection accuracy, and the performance of the sea ice detection algorithm was assessed at various window sizes (1 × 1, 3 × 3, 5 × 5, 7 × 7, and 9 × 9). The results indicate that larger window sizes improved the performance metrics, highlighting the importance of considering surrounding reflectance variations to enhance sea ice detection accuracy. Furthermore, the developed algorithm was applied to hourly GOCI-II imagery to evaluate sea ice detection performance. A qualitative evaluation confirmed that the algorithm successfully detected sea ice in the expected regions, and the results effectively captured the temporal movement of sea ice. In particular, as time progressed, the detected sea ice regions exhibited a southwestward drift due to tidal currents.

Future research will focus on developing a sea ice detection algorithm utilizing only the eight bands of GOCI. By integrating both GOCI and GOCI-II, it will be possible to conduct long-term sea ice detection, enabling the analysis of the relationship between climate change and sea ice

variations based on long-term time series data. This approach is expected to not only contribute to understanding long-term sea ice variation patterns but also provide a crucial foundation for investigating the impact of marine environmental changes on sea ice dynamics.

Acknowledgments

This work was supported by the Korea Institute of Marine Science & Technology Promotion (KIMST) funded by the Ministry of Oceans and Fisheries (20210046/RS-2021-KS211406, Development of marine satellite image analysis application technology) and the Korea Institute of Ocean Science & Technology (KIOST) research program (Grant no. PKA006C).

References

1 M. A. Tschudi, J. A. Maslanik, and D. K. Perovich: Remote Sens. Environ. **112** (2008) 2605. https://doi.org/10.1016/j.rse.2007.12.009
2 W. Shi and M. Wang: J. Mar. Syst. **95** (2012) 32. https://doi.org/10.1016/j.jmarsys.2012.01.012
3 J. Zheng, C. Ke, and Z. Shao: Acta Oceanolog. Sin. **36** (2017) 56. https://doi.org/10.1007/s13131-017-0993-3
4 X. Zhang, W. Dierking, J. Zhang, and J. Meng: IEEE J. Sel. Top. Appl. Earth Obs. Remote Sens. **8** (2014) 47. https://doi.org/10.1109/JSTARS.2014.2356552
5 C. Yue, J. Li, C. Guan, X. Lian, and K. Wu: J. Oceanol. Limnol. **37** (2019) 1857. https://doi.org/10.1007/s00343-019-8253-3
6 T. Li, D. Wu, R. Han, J. Xia, and Y. Ren: Comput. Mater. Continua **73** (2022) 3721. https://doi.org/10.32604/cmc.2022.029619
7 C. Liu, J. Chao, W. Gu, Y. Xu, and F. Xie: GISci. Remote Sens. **52** (2014) 115. https://doi.org/10.1080/15481603.2015.1007777
8 J. Karvonen, L. Shi, B. Cheng, M. Similä, M. Mäkynen, and T. Vihma: Remote Sens. **9** (2017) 234. https://doi.org/10.3390/rs9030234
9 W. Shi and M. Wang: J. Mar. Syst. **95** (2012) 41. https://doi.org/10.1016/j.jmarsys.2012.01.010
10 H. Su, Y. Wang, and J. Yang: Estuaries Coasts **35** (2011) 281. https://doi.org/10.1007/s12237-011-9425-3
11 S. Yuan, C. Liu, and X. Liu: Chin. Geogra. Sci. **28** (2018) 863. https://doi.org/10.1007/s11769-018-0986-y
12 Z. Wang, P. Sun, L, Wang, M. Zhang, and Z. Wang: J. Spectro. (2021). https://doi.org/10.1155/2021/9974845
13 W. Lang, Q. Wu, X. Zhang, J. Meng, N. Wang, and Y. Cao: J. Appl. Remote Sens. **8** (2013) 083650. https://doi.org/10.1117/1.JRS.8.083650
14 W. Liu, H. Sheng, and X. Zhang: Acta Oceanol. Sin. **35** (2016) 105. https://doi.org/10.1007/s13131-016-0910-1
15 H.-S. Lee and K.-S. Lee: J. Mar. Sci. Technol. **24** (2016) 1129. https://doi.org/10.6119/JMST-016-1026-1
16 Y. Yan, K. Huang, D. Shao, Y. Xu, and W. Gu: Sustainability **11** (2019) 777. https://doi.org/10.3390/su11030777
17 L. Ning, F. Xie, W. Gu, Y. Xu, S. Huang, S. Yuan, W. Cui, and J. Levy: Int. J. Remote Sens. **30** (2009) 4539. https://dx.doi.org/10.1080/01431160802592542
18 M. Madhiarasan and M. Louzazni: J. Electr: Comput. Eng. **2022** (2022) 5416722. https://doi.org/10.1155/2022/5416722
19 S. Chen, E. Xie, C. Ge, R. Chen, D. Ling, and P. Luo: IEEE Trans. Pattern Anal. Mach. Intell. **52** (2023) 12. https://doi.org/10.1109/TPAMI.2023.3303397
20 A. R. Marakhimov and K. K. Khudaybergenov: J. Math. Sci. **265** (2022) 43. https://doi.org/10.1007/s10958-022-06043-z
21 J. S. Hesthaven and S. Ubbiali: J. Comput. Phys. **363** (2018) 55. https://doi.org/10.1016/j.jcp.2018.02.037
22 C. Zhang, X. Pan, H. Li, A. Gardiner, I. Sargent, J. Hare, and P. M. Atkinson: ISPRS J. Photogramm. Remote Sens. **140** (2018) 133. https://doi.org/10.1016/j.isprsjprs.2017.07.014

About the Authors

Kwangseok Kim received his B.S. degree in biological education from Jeju National University, Jeju, Republic of Korea, in 2008 and his M.S. degree from the Interdisciplinary Postgraduate Program in Marine Meteorology of Jeju National University in 2012. Since 2012, he has been a researcher at the Korea Ocean Satellite Center (KOSC) of the Korea Institute of Ocean Science and Technology (KIOST). His research interests are in the application of ocean remote sensing.

Min-Kyu Kim received his B.S., M.S., and Ph.D. degrees from Korea Maritime & Ocean University, Republic of Korea, in 2016, 2018, and 2023, respectively. Since 2024, he has been a researcher at the Maritime Robotics Test & Evaluation Center of the Korea Institute of Ocean Science and Technology (KIOST). His research interests are in marine platform control and AI.

Young-Je Park received his B.S. degree from Seoul National University in 1988 and his M.S. and Ph.D. degrees from KAIST, Korea, in 1990 and 1998, respectively. After ocean-color-related experiences in Japan, Belgium, and Australia until 2010, he became involved in geostationary ocean color satellite projects at KIOST. Since 2024, he has been working at TelePIX Co., Ltd. as Chief Research Officer.

Hyun Yang received his B.S., M.S., and Ph.D. degrees in computer engineering from Chung-Ang University, Seoul, Korea in 2006, 2008, and 2012, respectively. He is working at the Korea Maritime and Ocean University as a professor. His research interests are in maritime AI and big data.

Hyeong-Tak Lee received his B.S. degree in nautical science from the Department of Maritime Transportation Sciences at Korea Maritime & Ocean University (KMOU), Busan, South Korea, in 2013 and his M.E. degree from the Graduate School of KMOU in 2019. In addition, he received his Ph.D. degree from the Ocean Science and Technology School, KMOU, in 2022. He worked for Hanjin Shipping Co., Ltd. as a navigating officer and worked for four years on container vessels. Moreover, he worked as an instructor and chief officer on the training ship "HANBADA" for 2.5 years. He is currently a senior research scientist at the Korea Institute of Ocean Science and Technology, Busan, South Korea. His research interests include marine artificial intelligence and data science.

Hee-Jeong Han received his B.S. degree from KAIST, Korea, in 1999 and his M.S. degree from Ajou University Graduate School of Information and Communication Technology, Korea, in 2010. From 2000 to 2005, he was a software developer at Pixoneer Geomatics, Korea. Since 2006, he has been a principal research specialist at KIOST. His research interests include ocean color remote sensing, optical sensors, parallel data processing, and AI analysis applications using satellite data.

Suk Yoon received her B.S. degree from Sangmyung University, Republic of Korea, in 2003 and her M.S. degree from Sung Kyun Kwan University in 2005. Since 1998, she has been a researcher at the Korea Ocean Satellite Center (KOSC) of the Korea Institute of Ocean Science and Technology (KIOST). Her research interests are in the application of ocean remote sensing.

Jeong-Eon Moon received his B.S. and M.S. degrees from Jeju National University, Republic of Korea, in 1995 and 2001, respectively, and his Ph.D. degree from Inha University, Republic of Korea, in 2005. Since 1998, he has been a scientist at KIOST. His research interests are in ocean color remote sensing, CAL/VAL of ocean satellite data, and in situ observation for ocean optics.